Dinuclear (d^3-d^3) Diolate Complexes of Molybdenum and Tungsten. 2.[1] Derivatives of 2,2′-Methylenebis(6-*tert*-butyl-4-methylphenoxide). Direct Observation of the Conversion of Bridged to Chelate Isomers (M = Mo) and Reversible Carbon−Hydrogen Bond Oxidative Addition (M = W)

Malcolm H. Chisholm,* Jui-Hsien Huang, John C. Huffman, and Ivan P. Parkin†

Department of Chemistry and Molecular Structure Center, Indiana University, Bloomington, Indiana 47405

Received November 27, 1996[⊗]

Hydrocarbon solutions of $Mo_2(NMe_2)_6$ and 2,2′-methylenebis(6-*tert*-butyl-4-methylphenol) (≥2 equiv), HO〰CH_2〰OH, yield $Mo_2(NMe_2)_2$(O〰CH_2〰O)$_2$, **I**, which exists in bridged **Ib** and chelated **Ic** isomers. These are formed under kinetic control, and recrystallization allows the separation of **Ib** (orange cubes) from **Ic** (yellow cubes) both of which have been crystallographically characterized. In each there is an ethane-like $O_2NMo{\equiv}MoO_2N$ core with Mo−Mo = 2.2 Å (average). In **Ib** the two O〰CH_2〰O ligands span the Mo≡Mo bond yielding a molecule of C_2 symmetry. In **Ic** the molecule has near-C_2 symmetry in the solid state, but in solution there is either rapid rotation about the M≡M bond or the anti-rotamer is preferred. In benzene-d_6, **Ib** and **Ic** do not interconvert at 110 °C over a period of days. However, the addition of pyridine or acetonitrile causes the isomerization of **Ib** to **Ic**, thereby establishing that **Ic** is the thermodynamic isomer. The rate of conversion of **Ib** to **Ic** has been shown to be dependent on the square of the concentration of added pyridine: $k_{obs} = k[py]^2$. From the temperature dependence of k_{obs}, we determine $\Delta H^{\ddagger} = 19\ (\pm 1)$ kcal/mol and $\Delta S^{\ddagger} = -25\ (\pm 3)$ eu for the pyridine-promoted isomerization of **Ib** to **Ic**. The related reaction involving $W_2(NMe_2)_6$ and HO〰CH_2〰OH (≥2 equiv) in hydrocarbon solvents at room temperature and below yields a dark brown crystalline compound, wherein C−H activation has occurred at one of the O〰CH_2〰O diolate ligands, $W_2(\mu\text{-H})(\mu\text{-NMe}_2)(NMe_2)(\eta^2\text{-O}〰CH_2〰O)(\eta^3\text{-O}〰CH〰O)(HNMe_2)$, **2**. The W−W distance in **2** is 2.495(1) Å, consistent with a $(W{=}W)^{8+}$ core. Heating **2** in the solid-state under a dynamic vacuum leads to the elimination of $HNMe_2$ and the formation of **3**, $W_2(NMe_2)_2(\eta^2\text{-O}〰CH_2〰O)_2$, an analog of **Ic**. In benzene-d_6 the equilibrium involving **2** and **3** + $HNMe_2$ has been observed by ^{1}H NMR spectroscopy. The addition of pyridine to hydrocarbon solutions of **3** yields $W_2(\mu\text{-H})(\mu\text{-NMe}_2)(\eta^2\text{-O}〰CH_2〰O)(\mu^3\text{-O}〰CH〰O)(NMe_2)$(py), **4**, which has been shown by single-crystal X-ray crystallography to be an analogue of **2**. Studies of the addition of PMe_3 to toluene-d_8 solutions of **3** at low temperatures reveal that adduct formation occurs prior to C−H oxidative addition. For the equilibrium involving **4** and **3** + py in benzene-d_6, $\Delta H^{\circ} = 14\ (\pm 1)$ kcal/mol and $\Delta S^{\circ} = 22\ (\pm 3)$ eu.

Introduction

The chelate effect in coordination chemistry has most pronounced kinetic and thermodynamic consequences.[2] In the chemistry of dinuclear complexes with M-M quadruple bonds bidentate phosphines have been used to obtain chelating and bridged isomers and their isomerizations have been studied with an aim to determine the operation of the internal flip mechanism, eq 1.[3,4]

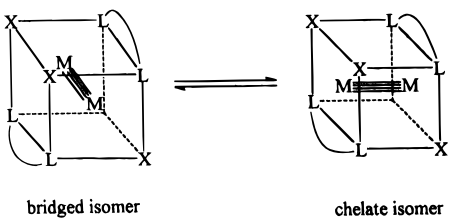

(1)

In the chemistry of d^3-d^3 ethane-like dinuclear complexes there is evidently a relatively high kinetic barrier to a related internal-flip of the M≡M unit within an octahedron of ligands since it has been known for some time that 1,2- and 1,1-isomers of the type shown below do not interconvert in solution even at elevated temperatures, eq 2.[5]

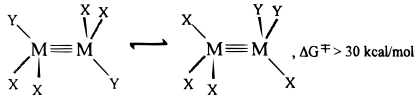

(2)

Chelating ligands have also been used to probe the nature of M−M bonding as a function of conformation, e.g. to probe the $\delta \rightarrow \delta^*$ transition as a function of twist from the eclipsed

† Present address: Department of Chemistry, Christopher Ingold Laboratories, University College London, 20 Gordon Street, London WC1 OAJ, England.

⊗ Abstract published in *Advance ACS Abstracts,* March 15, 1997.

(1) Part 1: Chisholm, M. H.; Parkin, I. P.; Folting, K.; Lobkovsky, E. *Inorg. Chem.* **1997**, *36,* 1636.

(2) (a) Basolo, F.; Pearson, R. G. *Mechanisms of Inorganic Reactions. A Study of Metal Complexes in Solution,* 2nd ed.; J. Wiley and Sons Publishers: New York, 1968. (b) Wilkins, R. G. *Kinetics and Mechanisms of Reactions of Transition Metal Complexes,* 2nd ed.; VCH Publishers: Weinheim, Germany, 1991.

(3) (a) Cotton, F. A.; Walton, R. A. Multiple Bonds Between Metal Atoms, 2nd ed.; Oxford University Press: Oxford, England, 1993. (b) Fraser, I. F.; McVitie, A.; Peacock, R. D. *J. Chem. Res. Synop.* **1984**, 420. (c) McVitie, A.; Peacock, R. D. *Polyhedron* **1992**, *11,* 2531. (d) Christie, S.; Fraser, I. F.; McVitie, A.; Peacock, R. D. *Polyhedron* **1986**, *5,* 35. (e) Agaskar, P. A.; Cotton, F. A. *Inorg. Chem.* **1986**, *25,* 15. (f) Cotton, F. A.; Kitagawa, S. *Polyhedron* **1988**, *7,* 463.

(4) Cayton, R. H.; Chisholm, M. H. *Inorg. Chem.* **1991**, *30,* 1422.

(5) (a) Chisholm, M. H.; Rothwell, I. P. *J. Chem. Soc., Chem. Commun.* **1980**, 985. (b) Chisholm, M. H.; Folting, K.; Huffman, J. C.; Rothwell, I. P. *Organometallics* **1982**, *1,* 251.

S0020-1669(96)01429-2 CCC: $14.00

conformation.[6] Similarly, the usually staggered ethane-like d^3-d^3 dinuclear complexes of type $X_3M{\equiv}MX_3$ (X = alkyl, NMe_2, OR, SR, SeR, etc.)[7] may be constrained to an eclipsed geometry through the use of chelating amide and pinacolate ligands as was shown for $M_2(MeNCH_2CH_2NMe)_3$[8] and $M_2(OCMe_2CMe_2O)_3$.[9]

In the previous paper,[1] we examined the ligation of the diolate derived from deprotonation of 2,5-dimethylhexane-2,5-diol (LH_2) at the $(M{\equiv}M)^{6+}$ center, where Mo = Mo and W. In the reaction between $M_2(NMe_2)_6$ compounds and LH_2, the kinetic products were $M_2(\eta^2\text{-L})_2(\mu\text{-L})(HNMe_2)_2$ which upon heating converted to $M_2(\mu\text{-L})_3$ compounds with the liberation of $HNMe_2$. The reversible equilibrium involving these two compounds in the presence of $HNMe_2$ was observed and was noted to have a significant kinetic barrier. The detailed matter of how chelate and bridging diolate ligands are interconverted in the presence of a Lewis base such as $HNMe_2$ was not established. We turned to the use of the diolate ligand derived from the deprotonation of 2,2′-methylenebis(6-*tert*-butyl-4-methylphenol), abbreviated hereafter to HO~~CH_2~~OH (**A**), and report here our findings.

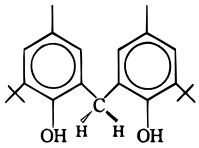

A

We are able to establish in some detail the nature of the interconversion of bridged and chelate isomers in the presence of Lewis bases and we have observed the first example of the reversible oxidative addition of a C-H bond to M-M multiple bonded complex.[10]

Results and Discussion

Synthesis. The reaction between $Mo_2(NMe_2)_6$ and HO~~CH_2~~OH (2 equiv or more) yields a compound of formula $Mo_2(NMe_2)_2(O\sim\sim CH_2\sim\sim O)_2$, **1**, which exists in two isomeric forms as described below. Only four of the six NMe_2 ligands are substituted even in the presence of an excess of the chelating diphenol, a fact we attribute to steric factors, eq 3.

$$Mo_2(NMe_2)_6 + 2HO\sim\sim CH_2\sim\sim OH \xrightarrow[\text{toluene}]{22\ ^\circ C} Mo_2(NMe_2)_2(O\sim\sim CH_2\sim\sim O)_2 + 4HNMe_2 \quad (3)$$

If reaction 3 is carried out in a hexane/ether solution, the product of crystallization is the bridged isomer **Ib**, $Mo_2(NMe_2)_2(\mu\text{-}O\sim\sim CH_2\sim\sim O)_2$, which forms orange cubes. The chelating isomer **Ic**, $Mo_2(NMe_2)_2(\eta^2\text{-}O\sim\sim CH_2\sim\sim O)_2$, can be separated as a yellow crystalline product by fractional crystallization in benzene wherein the less soluble isomer **Ib** is removed first. The total crystalline yield of **I** in reaction 3 is *ca*. 78%, but the isolated crystalline yield of **Ib** is 23% and **Ic**, 15%. Both isomers are thermally robust even at 110 °C and in the solid-state are relatively air-stable when compared to many metal amido complexes. Presumably, steric crowding by the hydrocarbon ligand prevents ease of access to the Mo−NMe_2 groups and the $(M{\equiv}M)^{6+}$ core by small molecules such as O_2, CO_2, CO, and even H_2O. NMR data are recorded in the Experimental Section, and the data are discussed later in terms of the solution behavior of these isomers.

The reaction between $W_2(NMe_2)_6$ and HO~~CH_2~~OH (≥2 equiv) in toluene or hexane proceeds according to eq 4 at room temperature or below, yielding $W_2(\mu\text{-H})(\mu\text{-}NMe_2)(\eta^2\text{-}O\sim\sim CH_2\sim\sim O)(\eta^3\text{-}O\sim\sim CH\sim\sim O)(NMe_2)(HNMe_2)$, **2**, which is obtained as a dark brown crystalline compound by cooling the mother liquor to *ca* −20 °C. However, if reaction 4 is carried out and the product of the reaction obtained by solvent removal

$$W_2(NMe_2)_6 + 2HO\sim\sim CH_2\sim\sim OH \xrightarrow[\text{hexane/toluene}]{0-22\ ^\circ C} W_2(\mu\text{-H})(\mu\text{-}NMe_2)(\eta^2\text{-}O\sim\sim CH_2\sim\sim O)(\eta^3\text{-}O\sim\sim CH\sim\sim O)(NMe_2)(HNMe_2) + 3HNMe_2 \quad (4)$$

under vacuum with heating, then the yellow-brown crystalline compound $W_2(NMe_2)_2(\eta^2\text{-}O\sim\sim CH_2\sim\sim O)_2$, **3**, is isolated in 60% recrystallized yield.

The conversion of **2** to **3** can be brought about by heating a solid sample of **2** under a dynamic vacuum or N_2 flow, and the addition of $HNMe_2$ to a benzene-d_6 solution of **3** can be seen to regenerate **2**. Thus, the equilibrium 5 has been established in solution.

$$\underset{\mathbf{2}}{W_2(\mu\text{-H})(\mu\text{-}NMe_2)(\eta^2\text{-}O\sim\sim CH_2\sim\sim O)(\eta^3\text{-}O\sim\sim CH\sim\sim O)(NMe_2)(HNMe_2)} \rightleftharpoons \underset{\mathbf{3}}{W_2(NMe_2)_2(\eta^2\text{-}O\sim\sim CH_2\sim\sim O)_2} + HNMe_2 \quad (5)$$

The conversion of **3** to a pyridine adduct related to **2** is accomplished by the addition of an excess of pyridine to a hexane suspension **3** as shown in eq 6.

$$\underset{\mathbf{3}}{W_2(NMe_2)_2(\eta^2\text{-}O\sim\sim CH_2\sim\sim O)_2} + py(\text{excess}) \xrightarrow[\text{hexane}]{22\ ^\circ C} \underset{\mathbf{4}}{W_2(\mu\text{-H})(\mu\text{-}NMe_2)(\eta^2\text{-}O\sim\sim CH_2\sim\sim O)(\eta^3\text{-}O\sim\sim CH\sim\sim O)(NMe_2)(py)} \quad (6)$$

Compound **4** is a dark hydrocarbon crystalline solid which as we show later exists in equilibrium with **3** and free pyridine when heated in solution.

Solid State and Molecular Structures. $Mo_2(NMe_2)_2(\mu\text{-}O\sim\sim CH_2\sim\sim O)_2$, Ib. A view of this bridged isomer is shown in Figure 1. This view looking down the M−M axis reveals how the nearly staggered ethane-like $NO_2W{\equiv}WNO_2$ core is maintained with the presence of the two μ-O~~CH_2~~O ligands that form 9-membered rings. The molecule has crystallographically imposed C_2 symmetry. There are therefore two distinct types of ^{t}Bu groups and *p*-Me groups. The NC_2 units of the dimethylamido ligands are aligned colinear with the M−M axis giving rise to proximal and distal N*Me* groups. Also as can be seen from an inspection of Figure 1 the methylene protons of each O~~CH_2~~O ligand are diastereotopic. Selected bond distances and bond angles are given in Table 1. The Mo−O distances, 1.92(1) Å (average) are slightly longer than those seen in $Mo_2(alkoxide)_6$ complexes, and the Mo−N distance 1.921(5) Å is shorter than that in $Mo_2(NMe_2)_6$.[11] These observations can be taken to imply greater NMe_2 π-to-Mo dπ bonding in **Ib** than in $M_2(NMe_2)_6$ and similarly that ArO^- ligands are poorer π-donors than alkoxides. The angles associated with the central $O_2NMo{\equiv}MoO_2N$ are unexceptional.

(6) See ref 3a, pp 192−193, and references therein.
(7) Chisholm, M. H. *Acc. Chem. Res.* **1990**, *23*, 419.
(8) Blatchford, T. P.; Chisholm, M. H.; Huffman, J. C *Inorg. Chem.* **1987**, *26*, 1920.
(9) Chisholm, M. H.; Folting, K.; Hampden-Smith, M. J.; Smith, C. A. *Polyhedron* **1987**, *6*, 1747.
(10) Preliminary reports on this work have appeared: (a) Chisholm, M. H.; Folting, K.; Lobkovsky, E.; Parkin, I. P.; Streib, W. E. *J. Chem. Soc., Chem. Commun.* **1991**, 1673. (b) Chisholm, M. H.; Huang, J.-H.; Huffman, J. C. *J. Organomet. Chem.*, in press.
(11) Chisholm, M. H.; Cotton, F. A.; Frenz, B. A.; Reichert, W. W.; Shive, L. W.; Stults, B. R. *J. Am. Chem. Soc.* **1976**, *98*, 4469.

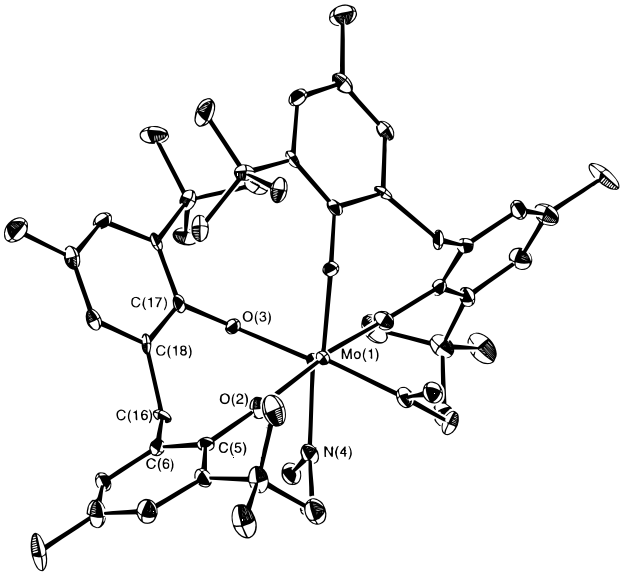

Figure 1. View of the molecular structure of **1b** showing the staggered conformation of the central $O_2NMo{\equiv}MoNO_2$ moiety.

Table 1. Selected Bond Distances (Å) and Angles (deg) for Compounds **1b**

Bond Distances			
Mo(1)−Mo(1)	2.245(1)	Mo(1)−N(4)	1.921(5)
Mo(1)−O(2)	1.915(4)	O(2)−C(5)	1.378(7)
Mo(1)−O(3)	1.921(5)	O(3)−C(17)	1.372(7)
Bond Angles			
Mo(1)−Mo(1)−O(2)	111.2(1)	Mo(1)−O(2)−C(5)	165.8(4)
Mo(1)−Mo(1)−O(3)	109.4(1)	Mo(1)−O(3)−C(17)	139.3(3)
Mo(1)−Mo(1)−N(4)	97.9(2)	Mo(1)−N(4)−C(28)	135.5(4)
O(2)−Mo(1)−O(3)	115.5(2)	Mo(1)−N(4)−C(29)	112.5(4)
O(2)−Mo(1)−N(4)	113.7(2)	C(28)−N(4)−C(29)	111.3(5)
O(3)−Mo(1)−N(4)	107.8(2)		

The Mo−O−C angles are 166° and 139°, the former being more typical for a M−O−C angle associated with a bulky aryloxide.[12]

$Mo_2(NMe_2)_2(\eta^2\text{-}O{\sim\sim}CH_2{\sim\sim}O)_2$, Ic. An ORTEP drawing of the chelated isomer is shown in Figure 2. Again this view of the molecule reveals the nearly perfectly staggered conformation of the $O_2NMo{\equiv}MoNO_2$ core which has virtual (but not crystallographically imposed) C_2 symmetry. Selected bond distances and bond angles are given in Table 2. The Mo−N distances of 1.91(1) Å (average) are again notably shorter than those in $Mo_2(NMe_2)_6$ and the Mo−O distances of 1.95(1) Å (average) longer than those associated with M−O (alkoxide) distances.[13] The chelates form eight-membered rings and the Mo−O−C angles again fall into two sets, one at 124° and the other at 114°, but both are much smaller than those seen in **Ib**. The $O{\sim\sim}CH_2{\sim\sim}O$ ligands are "roof" shaped and have their pitch directed away from the Mo_2 center as shown in Figure 3. Again the methylene protons are inequivalent with one being directed away from and the other being directed toward the Mo≡Mo bond. The view shown in Figure 3 also emphasizes that within the eight-membered ring the methylene carbon and the Mo atom are brought into relatively close proximity. The Mo(1)−C(10) and Mo(2)−C(35) distances are 3.11(1) and 3.12(1) Å, respectively. These can be compared with the Mo(1)−C(16) distances seen in the nine-membered ring in **Ib**, 3.59(1) Å. A comparison of the conformations in the eight- and nine-membered rings is also shown in Figure 3. In both rings one can see how the methylene carbon is directed toward the metal atoms. It is this close proximity that leads to facile C−H activation as described later. However, in the ground state we find no evidence from NMR (J_{CH} values) or IR data for the presence of an agostic M···H−C interaction (see Experimental Section).[14]

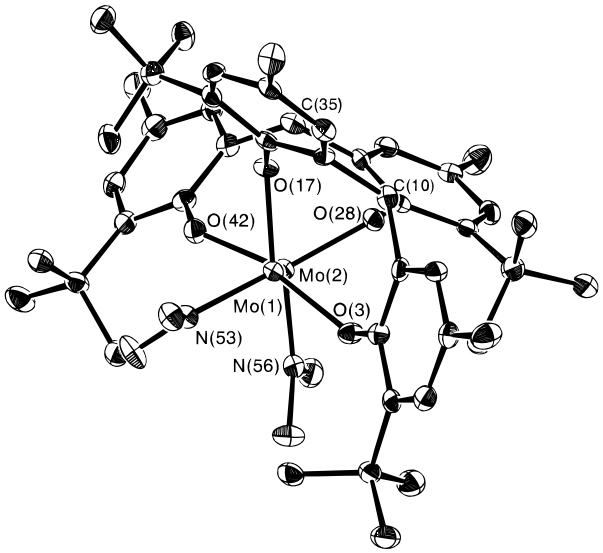

Figure 2. View of the molecular structure of **1c**, similar to that shown for **1b** in Figure 1, and showing the roof shape of the $O{\sim\sim}CH_2{\sim\sim}O$ ligand directed away from the Mo-Mo bond.

Table 2. Selected Bond Distances (Å) and Angles (deg) for Compound **1c**

Bond Distances			
Mo(1)−Mo(2)	2.216(1)	O(17)−C(16)	1.384(9)
Mo(1)−O(3)	1.954(5)	O(28)−C(29)	1.364(9)
Mo(1)−O(17)	1.947(3)	O(42)−C(41)	1.388(7)
Mo(1)−N(53)	1.907(5)	N(53)−C(54)	1.47(1)
Mo(2)−O(28)	1.953(4)	N(53)−C(55)	1.443(6)
Mo(2)−O(42)	1.951(6)	N(56)−C(57)	1.46(1)
Mo(2)−N(56)	1.915(5)	N(56)−C(58)	1.453(5)
O(3)−C(4)	1.378(7)		
Bond Angles			
Mo(2)−Mo(1)−O(3)	102.2(2)	O(42)−Mo(2)−N(56)	109.8(2)
Mo(2)−Mo(1)−O(17)	92.8(2)	Mo(1)−O(3)−C(4)	123.6(5)
Mo(2)−Mo(1)−N(53)	107.8(2)	Mo(1)−O(17)−C(16)	114.1(3)
O(3)−Mo(1)−O(17)	128.9(1)	Mo(2)−O(28)−C(29)	111.9(3)
O(3)−Mo(1)−N(53)	109.6(2)	Mo(2)−O(42)−C(41)	124.3(6)
O(17)−Mo(1)−N(53)	111.6(2)	Mo(1)−N(53)−C(54)	113.0(3)
Mo(1)−Mo(2)−O(28)	91.3(2)	Mo(1)−N(53)−C(55)	135.4(5)
Mo(1)−Mo(2)−O(42)	103.7(2)	C(54)−N(53)−C(55)	111.6(6)
Mo(1)−Mo(2)−N(56)	107.1(2)	Mo(2)−N(56)−C(57)	113.4(3)
O(28)−Mo(2)−O(42)	127.8(1)	Mo(2)−N(56)−C(58)	134.7(6)
O(28)−Mo(2)−N(56)	112.7(3)	C(57)−N(56)−C(58)	111.9(5)

$W_2(\mu\text{-}H)(\mu\text{-}NMe_2)(\eta^2\text{-}O{\sim\sim}CH_2{\sim\sim}O)(\eta^3\text{-}O{\sim\sim}CH{\sim\sim}O)(NMe_2)(HNMe_2)$, 2. A view of the molecular structure of compound **2** is shown in Figure 4. This view taken perpendicular to the W−W axis reveals that one of the diolate ligands has undergone cyclometallation so that W(1) forms two five-membered rings in the W(η^3-O~~CH~~O) moiety. The W(1)−C(10) distance is 2.21(1) Å, a typical $W-C_{sp^3}$ bond distance. The bridging hydride shown by the open circle in Figure 4 was not located crystallographically but is seen in the ^1H NMR spectrum (see later). There are two amide ligands, one bridging and one terminal denoted by N(53) and N(59), respectively, and one amine, Me_2NH, ligand denoted by N(56). The W−N distances of 1.90(2) (terminal amide), 2.13(1) and 2.09(1) (bridging amide), and 2.26(1) Å (terminal amine) are clearly distinct and allow an unequivocal assignment. Furthermore, the angles subtended at N(56) to W(1), C(57), and C(58) implying N_{sp^3} rather than N_{sp^2} hybridization. The W−W distance of 2.495(1)

(12) Coffindaffer, T. W.; Steffey, B. D.; Rothwell, I. P.; Folting, K.; Huffman, J. C.; Streib, W. E. *J. Am. Chem. Soc.* **1989**, *111*, 4742.
(13) Chisholm, M. H. *Polyhedron* **1983**, *2*, 681.
(14) Brookhardt, M. H.; Green, M. L. H. *J. Organomet. Chem.* **1983**, *250*, 395.

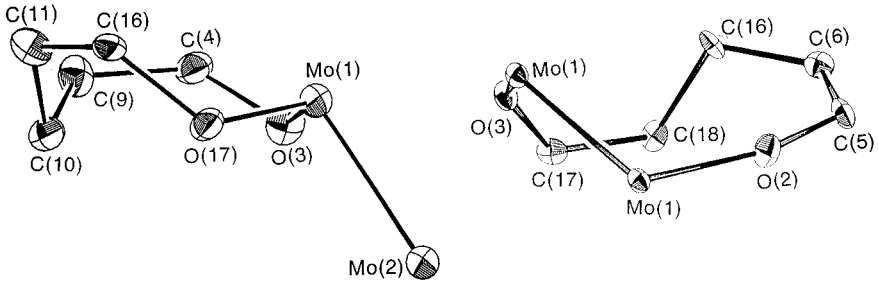

Figure 3. Comparison of the eight- and nine-membered rings in **1c** and **1b**, respectively. The methylene carbons are C(10) and C(16).

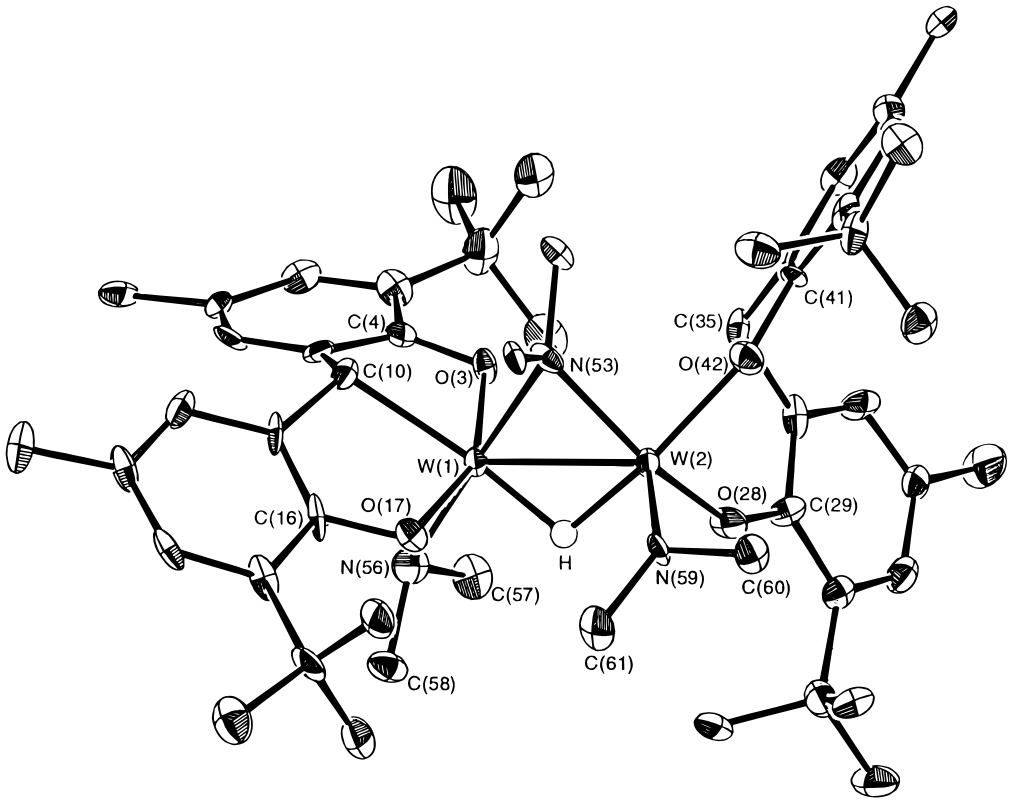

Figure 4. View of the molecular structure of compound **2** showing the η^3-O⁓CH⁓O ligand bound to W(1). The bridging hydride is represented by the open circle in an anticipated position.

Table 3. Selected Bond Distances (Å) for Compound **2**

W(1)−W(2)	2.4946(6)	O(28)−C(29)	1.33(1)
W(1)−O(3)	1.987(7)	O(42)−C(41)	1.36(1)
W(1)−O(17)	1.967(7)	O(62)−C(63)	1.33(2)
W(1)−N(53)	2.132(8)	O(62)−C(65)	1.41(2)
W(1)−N(56)	2.262(9)	N(53)−C(54)	1.48(1)
W(1)−C(10)	2.21(1)	N(53)−C(55)	1.49(1)
W(2)−O(28)	1.939(7)	N(53)−C(57)	1.51(1)
W(2)−O(42)	1.998(7)	N(56)−C(58)	1.49(1)
W(2)−N(53)	2.090(9)	N(59)−C(60)	1.47(1)
W(2)−N(59)	1.901(8)	N(59)−C(61)	1.46(1)
O(3)−C(4)	1.36(1)	W(1)−H(1)	1.6(1)
O(17)−C(16)	1.38(1)	W(2)−H(1)	1.6(1)

Table 4. Selected Bond Angles (deg) for Compound **2**

O(3)−W(1)−O(17)	155.2(3)	N(53)−W(2)−N(59)	103.8(4)
O(3)−W(1)−N(53)	89.6(3)	W(1)−O(3)−C(4)	115.5(6)
O(3)−W(1)−N(56)	85.3(3)	W(1)−O(17)−C(16)	120.7(6)
O(3)−W(1)−C(10)	77.6(3)	W(2)−O(28)−C(29)	148.7(7)
O(17)−W(1)−N(53)	96.6(3)	W(2)−O(42)−C(41)	148.4(7)
O(17)−W(1)−N(56)	89.4(3)	W(1)−N(53)−W(2)	72.4(3)
O(17)−W(1)−C(10)	78.5(3)	W(1)−N(56)−C(57)	111.3(7)
N(53)−W(1)−N(56)	173.9(3)	W(1)−N(56)−C(58)	115.2(6)
N(53)−W(1)−C(10)	88.8(4)	W(2)−N(59)−C(60)	117.2(6)
N(56)−W(1)−C(10)	93.3(4)	W(2)−N(59)−C(61)	132.9(7)
O(28)−W(2)−O(42)	89.7(3)	C(54)−N(53)−C(55)	107.4(8)
O(28)−W(2)−N(53)	151.8(3)	C(57)−N(56)−C(58)	107.9(9)
O(28)−W(2)−N(59)	104.1(3)	C(60)−N(59)−C(61)	109.0(8)
O(42)−W(2)−N(53)	86.7(3)	W(1)−H(1)−W(2)	102.0(7)
O(42)−W(2)−N(59)	105.0(3)		

Å is typical of that associated with a $(W{=}W)^{8+}$ moiety[13] in confirmation of the C−H oxidative addition to the $(W{\equiv}W)^{6+}$ center. Excepting the W−W double bond the coordination about W(1) can be viewed to be derived from a distorted octahedron with O(17), C(10), and O(3) forming a meridinal ligation with the O(17)−W(1)−O(3) angle being 165°. Similarly, the amine and μ-amide ligands are trans with the N(56)−W(1)−N(53) angle = 174°. The coordination number for W(2) is five, and it is noteworthy that O(42)−W(2)−O(28) = 89.7(3)° and N(53)−W(2)−O(42) = 87.7(3)° while the angles N(59)−W(2) to O(42), O(28), N(53) are *ca.* 104°. Thus, while the hydride ligand is not located crystallographically it seems likely that the coordination geometry can be described as square pyramidal with the W(2)−N(59) (amide) bond in the apical position. Selected bond distances for **2** are given in Table 3 and selected bond angles in Table 4.

$W_2(\mu$-H)(μ-NMe_2)(η^3-O⁓CH⁓O)(η^2-O⁓CH_2⁓O)(NMe_2)(py), 4. A view of this molecule is given in Figure 5 which reveals its close similarity to that of **2** described above. The metric parameters are also very similar as revealed in Tables 5 and 6. Basically pyridine in **4** substitutes for the $HNMe_2$ ligand in **2**.

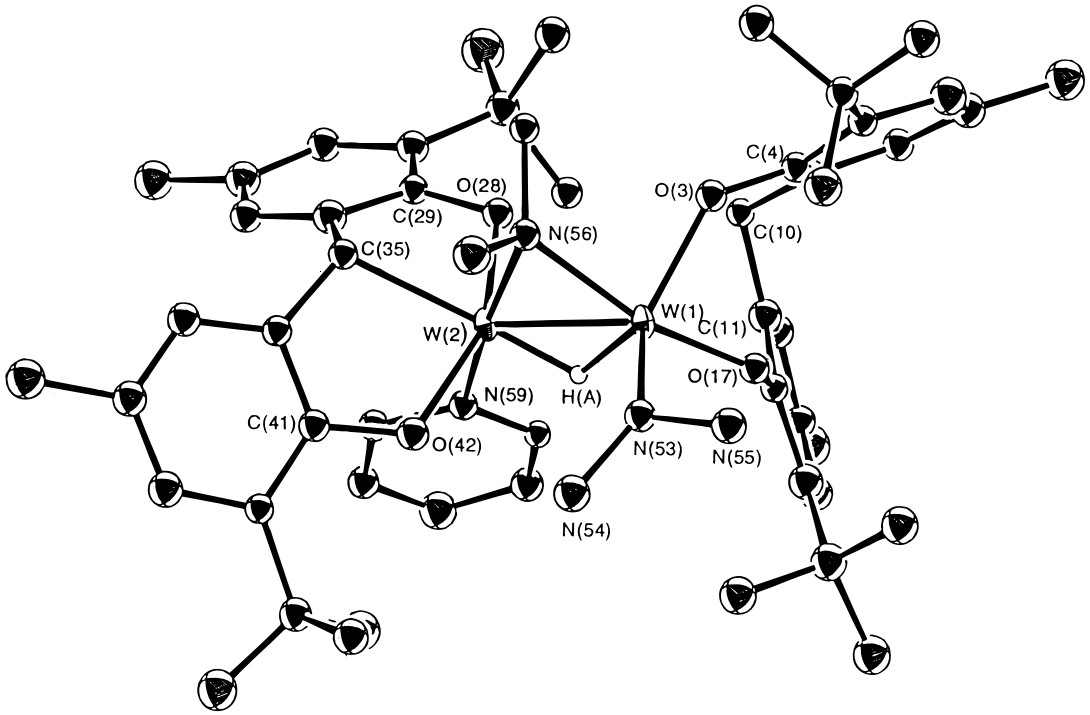

Figure 5. View of the molecular structure of compound **4** showing its close relationship to that of compound **2**.

Table 5. Selected Bond Distances (Å) for Compound **4**

W(1)−W(2)	2.470(1)	W(2)−N(59)	2.23(1)
W(1)−O(3)	2.00(1)	W(2)−C(35)	2.24(2)
W(1)−O(17)	1.94(2)	N(53)−C(54)	1.48(1)
W(1)−N(53)	1.87(1)	N(53)−C(55)	1.50(2)
W(1)−N(56)	2.14(2)	N(56)−C(57)	1.48(2)
W(2)−O(28)	1.95(1)	N(56)−C(58)	1.47(3)
W(2)−O(42)	1.99(1)	W(1)−H(A)	1.57(1)
W(2)−N(56)	2.15(1)	W(2)−H(A)	1.48(1)

Table 6. Selected Bond Angles (deg) for Compound **4**

O(3)−W(1)−O(17)	86.4(6)	W(2)−O(28)−C(29)	113.2(8)
O(3)−W(1)−N(53)	122.9(4)	W(2)−O(42)−C(41)	118(1)
O(3)−W(1)−N(56)	82.2(6)	W(1)−N(53)−C(54)	115.1(9)
O(17)−W(1)−N(53)	98.2(7)	W(1)−N(53)−C(55)	136.1(6)
O(17)−W(1)−N(56)	162.1(5)	C(54)−N(53)−C(55)	109(1)
N(53)−W(1)−N(56)	99.6(7)	W(1)−N(56)−W(2)	70.4(7)
O(28)−W(2)−O(42)	152.5(3)	C(57)−N(56)−C(58)	107(2)
O(28)−W(2)−N(56)	90.3(5)	W(1)−H(A)−W(2)	108(2)
O(28)−W(2)−N(59)	82.7(5)	O(3)−W(1)−H(A)	138(2)
O(28)−W(2)−C(35)	79.0(6)	O(17)−W(1)−H(A)	90(2)
O(42)−W(2)−N(56)	104.3(5)	N(53)−W(1)−H(A)	99(3)
O(42)−W(2)−N(59)	84.6(5)	N(56)−W(1)−H(A)	90(2)
O(42)−W(2)−C(35)	79.5(7)	O(28)−W(2)−H(A)	107.0(4)
N(56)−W(2)−N(59)	170.7(4)	O(42)−W(2)−H(A)	95.9(5)
N(56)−W(2)−C(35)	84.1(6)	N(56)−W(2)−H(A)	91.5(5)
N(59)−W(2)−C(35)	100.5(6)	N(59)−W(2)−H(A)	84.7(5)
W(1)−O(3)−C(4)	131(2)	C(35)−W(2)−H(A)	172.7(3)
W(1)−O(17)−C(16)	133.8(8)		

NMR Characterization of the New Compounds. The bridged compound $Mo_2(NMe_2)_2(\mu\text{-}O\sim\sim CH_2\sim\sim O)_2$, **Ib**, which has C_2 symmetry in the solid state (Figure 1) maintains this in solution. The most characteristic feature of the ^{1}H NMR spectra is the presence of two ^{t}Bu and two Me groups associated with the O~~CH_2~~O ligands, irrespective of temperature in the range 20−105 °C. The methylene O~~CH_2~~O protons appear as two doublets at 6.02 and 3.44 ppm with the former being the proton being directed toward the Mo≡Mo bond. The temperature invariance of the methylene CH_aH_b signals implies a certain degree of conformational rigidity; *i.e*. the 9-membered ring is not inverting rapidly and the positioning of the H_a and H_b protons and the methylene carbon are relatively fixed as indicated in Figure 3. The *NMe* resonances also appear as two singlets, δ 4.23 and 2.87 at 22 °C, and only at 105 °C in toluene-d_8 is there evidence for line broadening of these signals. Thus, there is a significant barrier, $\Delta G^{\ddagger} > 16$ kcal/mol, for rotation about the Mo−N bonds.

The chelated isomer **Ic** and $W_2(NMe_2)_2(O\sim\sim CH_2\sim\sim O)_2$ have very similar spectra and in contrast to **Ib** there is only one type of tBu and one type of Me signal associated with the O~~CH_2~~O ligand even at −80 °C in toluene-d_8. Thus on the NMR time scale anti ⇌ gauche isomerization must be facile (or the anti rotamer is favored in solution). The methylene protons of the O~~CH_2~~O ligands give rise to two doublets at *ca*. 4.5 and 3.7 ppm ($J_{HH} \sim 15$ Hz) corresponding to proximal and distal CH protons with respect to the M≡M bond. At room temperature the NMR resonances are also frozen out and give rise to two singlets from proximal and distal groups. No significant change in spectra was observed on raising the temperature to 110 °C in benzene-d_6. Again the temperature invariance of the methylene CH_aH_b resonances implies a certain rigidity of the 8-membered ring (Figure 3).

The ^{1}H NMR spectra associated with the hydrido bridged compounds **2** and **4** are complex but reveal the loss of symmetry of the molecules. There are four tBu groups and four Me groups arising from the η^2-O~~CH_2~~O and η^3-O~~CH~~O ligands, for example, in addition to ^{1}H signals arising from four aromatic groups. Data are given in the Experimental Section. However, the characteristic feature of these spectra is the hydride signal that appears at *ca*. 11.5 ppm, far downfield of the protio impurity signals of benzene-d_6 or toluene-d_8. This signal consists of a central resonance flanked by two sets of satellites arising from coupling to two chemically different ^{183}W nuclei, $I = {}^1/_2$, 14.5% natural abundance. The hydride signals for compound **4** are shown in Figure 6.

Isomerization of Ib to Ic. From the NMR characterization of **Ib** and **Ic** described above, it is apparent that in solution they do not interconvert even at 100 °C. Their formation in eq 3 is apparently under kinetic control. However, we have found that the addition of pyridine or acetonitrile to hydrocarbon solutions of **Ib** promotes isomerization to **Ic**, thereby establishing that **Ic** is the thermodynamic isomer.

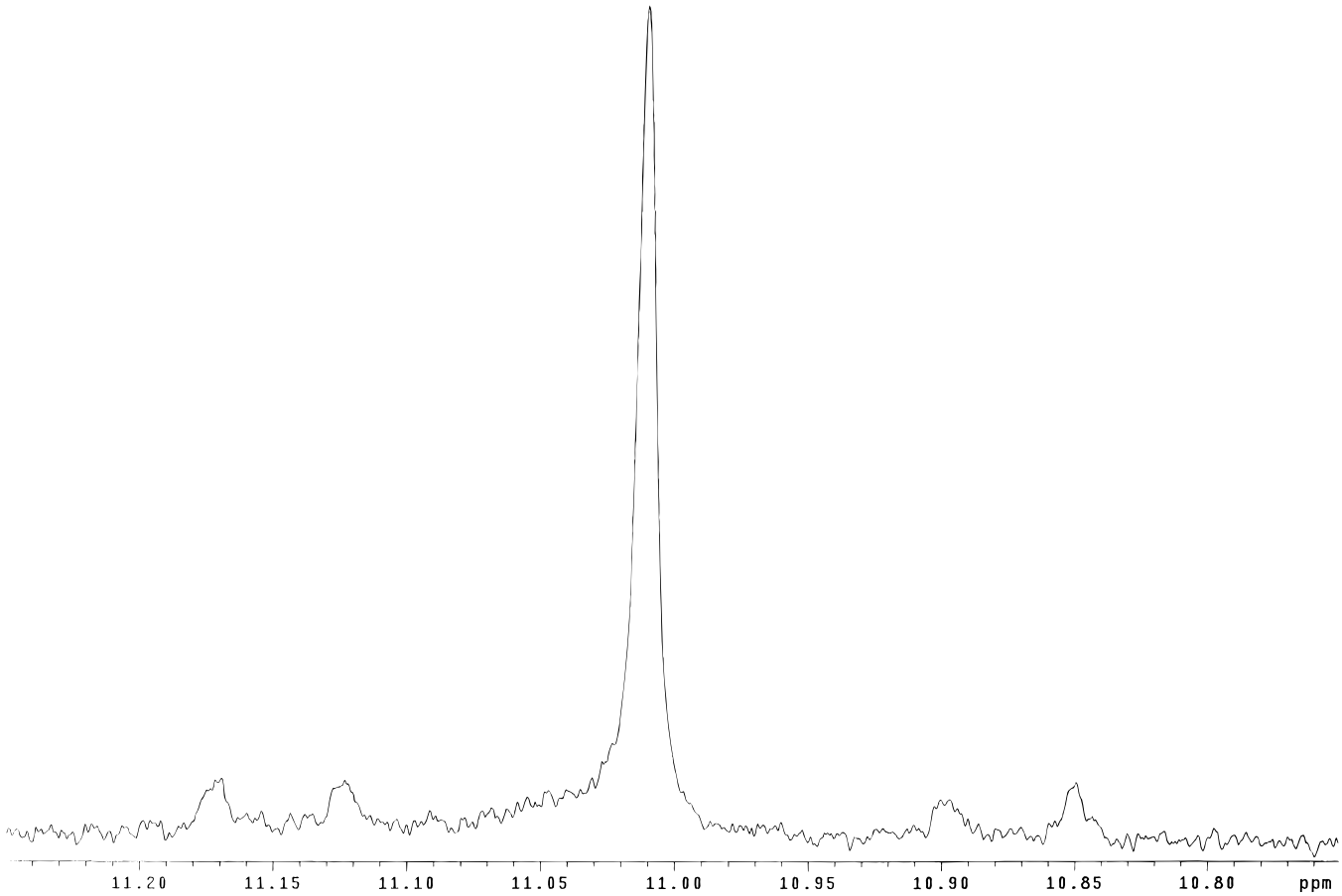

Figure 6. $W_2(\mu$-H) signal in the ^{1}H NMR spectrum of **2** showing the central signal flanked by satellites due to coupling to two inequivalent ^{183}W nuclei ($I = {}^1/_2$, 14.5% natural abundance).

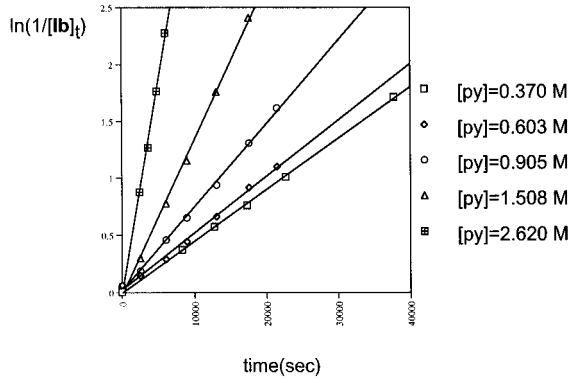

Figure 7. Plots of ln(1/[**1b**]$_t$) *vs* time with varying concentration of py during the isomerization **1b** → **1c**.

We have studied the conversion of **Ib** to **Ic** in benzene as a function of temperature, at 75−110 °C, and concentration of pyridine, from 0.37 to 2.62 M, where the [py] concentration is in excess of [**Ib**]. A plot of ln(1/[Ib]) *vs* time (s) as a function of [py] is shown in Figure 7. Assuming the kinetic rate law for the interconversion of **Ib** to **Ic** shown in eq 7, we see from

$$-\mathrm{d}[\mathbf{Ib}]/\mathrm{d}t = k[\mathbf{Ib}]^x[\mathrm{py}]^y = k_{\mathrm{obs}}[\mathbf{Ib}]^x \qquad (7)$$

Figure 7 that the rate is dependent on the concentration of pyridine. For a given concentration of **Ib** = 0.021 M, we have obtained k_{obs} as a function of [py]. See Table 7. A plot of k_{obs} *vs* [py]^2 yields a straight line, thereby establishing the order of the reaction in [py] as 2. The fact that the plots of ln(1/[Ib]) *vs* time with varying pyridine concentrations are linear (Figure 7) indicates that reaction 7 is first order in **Ib**. Thus in the pyridine-promoted isomerization of **Ib** to **Ic**, two molecules of pyridine

Table 7

[pyridine] (M)	k_{obs} (s^{-1})
2.620	3.73×10^{-4}
1.518	1.36×10^{-4}
0.905	7.32×10^{-5}
0.602	4.96×10^{-5}
0.370	4.52×10^{-5}

are present in the activated complex. With this in mind, it is interesting to speculate upon the geometry of the reactive intermediate or transition state. In benzene-d_6, it seems unlikely that Mo−O or Mo−N bond homolysis or heterolysis is occurring under such mild conditions. We propose that the presence of two pyridine ligands facilitates the formation of a symmetrical bridged complex as shown in eq 8.

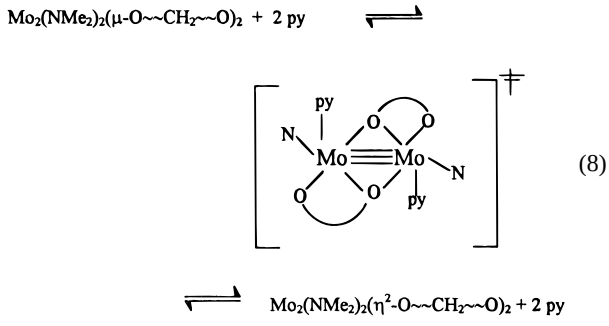

(8)

It may be noted that a structure similar to that shown in eq 8 for the activated complex is seen in the structure of $[Zr(O\sim\sim CH_2\sim\sim O)_2]_2$, which has two chelate $O\sim\sim CH_2\sim\sim O$ ligands and two η^1-μ-$O\sim\sim CH_2\sim\sim O$ ligands.[15]

(15) Chisholm, M. H.; Huang, J.-H.; Streib, W. E. *Polyhedron*, in press.

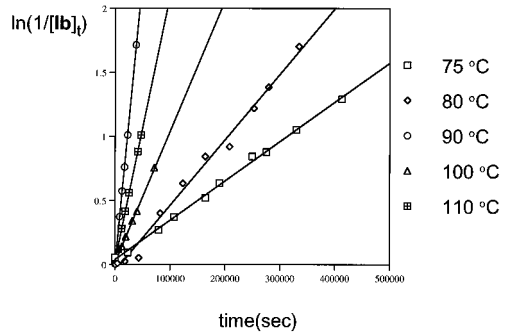

Figure 8. Plots of $\ln(1/[\mathbf{1b}]_t)$ *vs* time as a function of various temperatures but at a constant [py].

Table 8

T (°C)	k_{obs} (s^{-1})	$k = k_{ob}/[py]^2$
75	3.07×10^{-6}	2.24×10^{-5}
80	5.12×10^{-6}	3.74×10^{-5}
90	1.03×10^{-5}	7.49×10^{-5}
100	2.09×10^{-5}	1.53×10^{-4}
110	5.42×10^{-5}	3.30×10^{-4}

From studies of the conversion of **Ib**, 0.021 M, with [py] = 0.370 M as a function of temperature (75−110 °C) we can obtain k_{obs} as shown in Figure 8 and from this deduce k since $k = k_{obs}/[py]^2$. These values of k_{obs} and k are shown in Table 8 and from the Eyring plot of $\ln(k/T)$ *vs* $1/T$ we obtain the activation parameters $\Delta H^{\ddagger} = 19$ (±1) kcal/mol and $\Delta S^{\ddagger} = -25$ (±3) eu. The value of $\Delta S^{\ddagger}$ is perhaps relatively small in magnitude for a reaction that is second order in pyridine. Within this context it is worthwhile comparing it to studies of the equilibrium shown in eq 9 for monodentate alkoxides, *e.g.* R

$$M_2(OR)_6 + 2CH_3C{\equiv}N \rightleftharpoons Mo_2(OR)_6(CH_3CN)_2 \qquad (9)$$

$= CMe_2CF_3$,[16] for which the values of $\Delta H^{\circ} \sim -25$ kcal/mol and $\Delta S^{\circ} \sim -84$ eu have been determined along with the activation parameters $\Delta H^{\ddagger} \sim 19$ kcal/mol and $\Delta S^{\ddagger} \sim -35$ eu.[17] Thus, in the pyridine promoted isomerization of **Ib** to **Ic** it may well be that the loss in entropy in accessing the activated complex rests primarily with the uptake of the first equivalent of pyridine and the accompanying reorganization of ligands. To try to state more on the basis of the present findings would be unwise.

Studies of the Reversible C−H Bond Oxidative Addition to the $(W{\equiv}W)^{6+}$ Center. The equilibrium involving **2** and **3** + $HNMe_2$, eq 5, in benzene-d_6 and toluene-d_8 has already been noted as has the addition of pyridine to **3** to yield the CH activated complex **4**, eq 6. The reversibility of eq 5 has been studied through numerous cycles and the equilibrium involving pyridine, eq 6, has been monitored carefully as a function of temperature by NMR spectroscopy. From integrations of the methylene signals associated with the O⁓CH_2⁓O chelate in **4** with those of the two O⁓CH_2⁓O chelates in **3**, we have monitored the equilibrium in eq 6 in benzene-d_6 (**3** + py = **4**) as a function of temperature and determined the values of K_{eq} (see Experimental Section), which in turn yielded the thermodynamic parameters $\Delta H^{\circ} = -14$ (±1) kcal/mol and $\Delta S^{\circ} = -22$ (±3) eu. Thus, we see that the oxidized product **4** is favored on enthalpic grounds but disfavored by entropy.

A key question that then arises concerns the role of pyridine (or amine) in the C−H activation process. Does C−H oxidative addition occur prior to Lewis base uptake? If so, the role of the Lewis base may be viewed as merely stabilizing or trapping the product. Alternatively does Lewis base association promote C−H oxidative addition? In this scenario the Lewis base would be associated with the W_2 center first.

In order to interrogate this aspect of the reaction sequence, we turned to the use of tertiary phosphines as Lewis bases since both ^{31}P and ^{1}H NMR spectroscopy could be brought to bear on the problem. PPh_3 was found not to react with $W_2(NMe_2)_2(O{\sim}CH_2{\sim}O)_2$, **3**, in benzene-$d_6$, a fact we attribute to steric crowding with this rather bulky PR_3 ligand. However, PMe_3 did react with **3** in toluene-d_8, and we monitored the reaction from −70 to +70 °C. At low temperatures there is a color change of the yellow-brown **3** in toluene-d_8 to green in the presence of PMe_3. By ^{31}P NMR, free PMe_3 is seen at −60 ppm and a new signal *ca.* 0 ppm is present and assignable to a W−PMe_3 moiety. When the temperature is raised to −20 °C, little change is observed, but between −20 and +20 °C a new ^{31}P signal grows in at *ca.* −10 ppm flanked by ^{183}W, $I = {}^1/_2$, satellites. This resonance grows as the one at *ca.* 0 ppm disappears, and in the ^{1}H NMR spectrum a hydride signal grows in concomitantly at δ *ca.* 12.5 ppm. This is shown in Figure 9 where the hydride ligand can be seen to show coupling to ^{31}P and two inequivalent ^{183}W nuclei. The structure of this compound is thus considered to be related to that of **2** and **4** with PMe_3 in place of the nitrogen base. From these studies, we propose that Lewis base association occurs prior to C−H oxidative addition, and indeed the role of the Lewis base is to promote C−H oxidative addition by coordination to the ditungsten center.

Comparisons with Earlier Studies. The lack of the isomerization of **Ib** to **Ic** in toluene solution at 100 °C parallels the previous observation that 1,1- and 1,2-$Mo_2(NMe_2)_2(CH_2SiMe_3)_4$ isomers do not interconvert even upon heating to 100 °C in solution.[5] As shown in Figure 10 a series of internal flips of an M_2 unit within a pseudooctahedral N_2O_4 core would lead to the interconversion of 1,1-$M_2(\mu\text{-}O{\sim}CH_2{\sim}O)(\eta^2\text{-}O{\sim}CH_2{\sim}O)(NMe_2)_2$, **Ib** and **Ic** isomers. The transition state for such an internal flip involves two four-coordinate metal atoms in a distorted tetrahedral environment.[4] As we have shown previously, such an internal flip of an M_2 unit within an octahedron is not symmetry forbidden though M−M bonding is sacrificed in the transition state as indeed it is for an internal flip of a $M^{\underline{4}}M$ unit within a cube.[4] To compensate for the weakening of the M−M bonding, four bridged bonds are formed from two terminal bonds as shown in eq 10. That we observed no

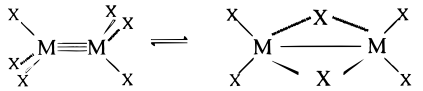

(10)

isomerization of **Ib** to **Ic** at 110 °C over a period of 2 days in toluene-d_8 reveals that the E_{Act} for eq 10 must be greater than 30 kcal/mol. A bridged isomer or transition state would be favored by groups that prefer bridging to terminal modes of bonding, and in this regard we mention that only for $W_2(NMe_2)_4(PR_2)_2$[18] and $W_2(O^tBu)_4(PR_2)_2$[19] have we ever seen bridged isomers (μ-PR_2) and even here the opening and closing of bridges is relatively slow; e.g. for $W_2(PCy_2)_2(NMe_2)_4 \rightarrow W_2(NMe_2)_4(\mu\text{-}PCy_2)_2$, $\Delta H^{\ddagger} \sim 19$ kcal/mol and $\Delta S^{\ddagger} \sim -12$ eu.[18] The bridged isomers have a puckered $W_2(\mu\text{-}P)_2$ core so as to maximize M−M bonding in the presence of the bridging phosphido ligands.

In our present study we have shown that the presence of a donor ligand, namely MeCN or py, facilitates the isomerization

(16) Freudenberger, J. H.; Pederson, S. F.; Schrock, R. R. *Bull. Chim. Soc. Fr.* **1985**, 349.
(17) Budzichowski, T. A.; Chisholm, M. H.; Tiedtke, D. Results to be published.
(18) Buhro, W. E.; Chisholm, M. H.; Folting, K.; Huffman, J. C.; Martin, J. D.; Streib, W. E. *J. Am. Chem. Soc.* **1988**, *10*, 6563.
(19) Buhro, W. E.; Chisholm, M. H.; Folting, K.; Eichhorn, B. W.; Huffman, J. C. *J. Chem. Soc., Chem. Commun.* **1987**, 845.

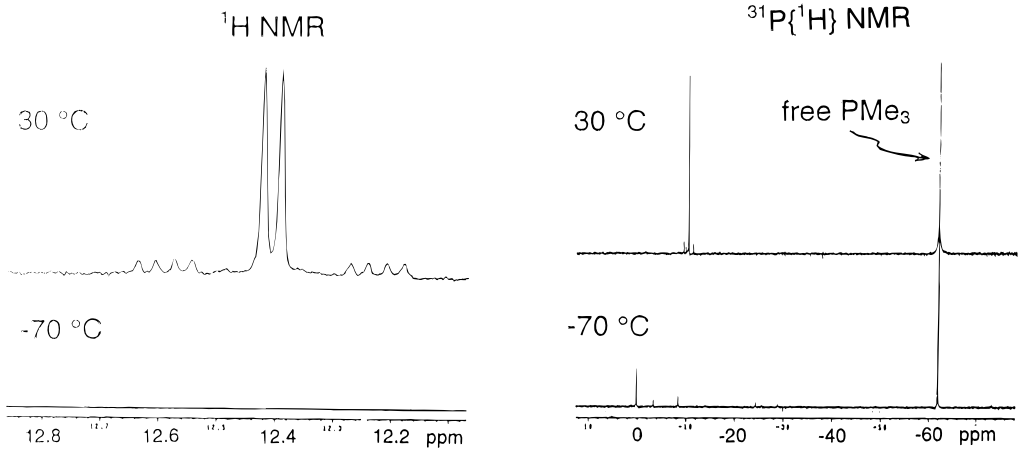

Figure 9. ^{1}H and ^{31}P{^{1}H] NMR spectra recorded during the reaction between **2** and PMe_3 in toluene-d_8. At −70 °C, there is evidence for PMe_3 adduct formation but no evidence of μ-H formation. At 30 °C, the μ-H signal shows both coupling to ^{31}P and two different ^{183}W nuclei. The PMe_3 bound ligand reveals coupling to ^{183}W.

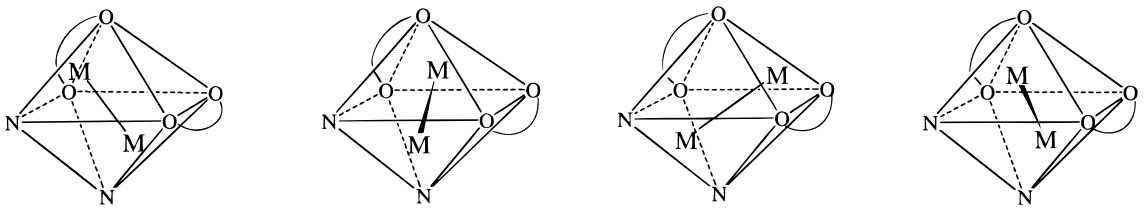

Figure 10. Four possible internal flips for a M_2 unit within an octahedral $M_2(O\sim\sim O)_2$ unit showing the conversion of the various isomers including the isomerization **1b** to **1c**.

of **Ib** to **Ic**, and furthermore from the kinetic studies this reaction requires 2 equiv of pyridine. It therefore seems that the increased coordination number and the formation of two new metal ligand bonds facilitates bridge formation; *i.e.*, the enthalpy of the formation of two M−py bonds compensates for the loss of M−M bonding. The proposed geometry for $Mo_2(NMe_2)_2(O\sim\sim CH_2\sim\sim O)_2(py)_2$ is shown in eq 8 and involves the fusing of two five-coordinate Mo atoms along a common edge. This allows us to return to the nature of the reaction involving the $M_2(diolate)_3$ complexes and $HNMe_2$ where the diolate is $OCMe_2CH_2CH_2CMe_2O$, eq 11. Here no isomer $M_2(\eta^2$-$OCMe_2CH_2CH_2CMe_2O)(\mu$-$OCMe_2CH_2CH_2CMe_2O)$ was seen and it seems likely now that the μ-to-η^2-diolate transformation requires the precoordination of two $HNMe_2$ ligands since the alternative intimate mechanism for **11** would involve a preequilibrium via the internal flip (Figure 10) followed by uptake of $HNMe_2$. Given that the internal flip involves a relatively high energy transition state, then the sluggish uptake of $HNMe_2$ in eq 11 follows from the requirement that its coordination promote the isomerization as we have seen for pyridine in the present study. However, for the larger and more bulky 2,2′-methylenebis(6-*tert*-butyl-4-methylphenoxide) ligands the pyridine adduct is not stable (kinetically persistent).

$$M_2(\mu\text{-}OCMe_2CH_2CH_2CMe_2O)_3 + 2HNMe_2 \rightleftharpoons M_2(\mu\text{-}OCMe_2CH_2CH_2CMe_2O)(\eta^2\text{-}OCMe_2CH_2CH_2CMe_2O)_2(HNMe_2)_2 \quad (11)$$

One might well wonder why the chelate isomer **1c** is thermodynamically favored over the bridged isomer **1b**. Given that both allow for the attainment of an ethane-like $NO_2M{\equiv}MO_2N$ skeleton of relatively undistorted proportions when compared to related $(M{\equiv}M)^{6+}$-containing compounds, one might be led to believe that ring-strain or intraligand repulsion interactions are responsible for the thermodynamic preference of **1c** over **1b**. We have performed simple molecular mechanics calculations (PC MODEL version 4.0—the MMX force field included π atoms, and the minimization included a normal RHF and full VESCF π atom calculations). In contrast to our expectations, the energy of **1c** is calculated to be higher than that of **1b** in the ground state structures obtained from the X-ray coordinates. The structures were then allowed to attain their minimum energy based on steric factors resulting in a considerable lowering of energy: −70 kcal/mol for **1c** *vs* −138 kcal/mol for **1b**. The minimized energy structures contained NC_2 units perpendicular to the M−M axis, which is not favorable on electronic grounds. From this we conclude that electronic factors, not steric factors, are responsible for the preference for **1c** over **1b**, but this matter remains under investigation.

In the chemistry of tungsten we see that the uptake of $HNMe_2$ or pyridine by **3**, $[W_2(\eta^2\text{-}O\sim\sim CH_2\sim\sim O)_2(NMe_2)_2]$, promotes the intramolecular C−H oxidative addition to the $(W{\equiv}W)^{6+}$ center. That this should occur for M = W but not M = Mo is understandable in terms of the relative ease of oxidation to $(M{\equiv}M)^{6+}$ moiety which is now well established to be easier for the third row than the second row element.[2a,20] Again the likely scenario is that pyridine uptake promotes bridge formation with destabilization of the M−M bonding orbitals, and this in turn facilitates the activation of a C−H bond which is by necessity in close proximity to the dinuclear center. (Note: no agostic W- - -H−C interaction was observed for **3**.) In this regard dinuclear chemistry is different from mononuclear chemistry since ligand loss, Lewis base dissociation, invariably promotes oxidative addition at mononuclear centers.[21] Indeed, the presence of excess Lewis base generally suppresses oxidative addition at mononuclear centers.

It should be noted that C−H activation at dinuclear centers has been seen previously as in the case of PPh_3 ligands at Rh_2^{4+}

(20) Chisholm, M. H. *Polyhedron* **1986**, *5*, 25.
(21) (a) Collman, J. P.; Hegedus, L. S.; Norton, J. R.; Finke, R. G. *Principles and Applications of Organotransition Metal Chemistry*; University Science Books: Mill Valley, CA, 1987. (b) Crabtree, R. H. *The Organometallic Chemistry of the Transition Metals*, 2nd ed.; J. Wiley and Sons Publishers: New York, 1993.

centers[22] and in the Na/Hg reduction of $W_2Cl_2(silox)_4$, where silox is OSi^tBu_3.[23] However, to our knowledge this is the first example of reversible C−H oxidative addition to a M−M multiple bond that has been directly monitored.

Experimental Section

All reactions and manipulations were carried out in a glovebox or Schlenk line under a nitrogen atmosphere. Solvents were dried by distillation over Na dispersion/benzophenone under a nitrogen atmosphere. ^{1}H and ^{13}C NMR spectra were recorded on a Varian XL-300 NMR spectrometer and referenced to the residual protio impurities of the deuterated solvent. $M_2(NMe_2)_6$ compounds were prepared as described elsewhere.[24] 2,2′-Methylenebis(6-*tert*-butyl-4-methylphenol) was purchased from Pfaltz and Bauer.

$Mo_2(NMe_2)_2(O\sim\sim CH_2\sim\sim O)_2$, I. A 30 mL Schlenk flask was charged with $Mo_2(NMe_2)_6$ (0.33 g, 0.72 mmol) and 2,2′-methylene-bis(6-*tert*-butyl-4-methylphenol) (0.49 g, 1.44 mmol). To the mixture was added 25 mL of hexane, and the resultant solution was stirred for 8 h; then the volatile components were removed under a dynamic vacuum. The residue was washed with 10 mL of cold hexane in two portions and then dried in vacuum. A mixture of **Ib** and **Ic** was isolated in 78% yield (0.53 g). The two isomers were then separated via fractional recrystallization in benzene. Pure **Ib** (0.154 g, 23% yield, based on Mo) and **Ic** (0.10 g, 15%) were obtained. ^{1}H NMR for **Ib** (δ, C_6D_6): 7.32 (s, aromatic protons, 4H), 7.22 (s, aromatic protons, 2H), 7.04 (s, aromatic protons, 2H), 6.02 (d, $^2J_{HH}$ = 15 Hz, methylene, 2H), 4.23 (s, N*Me*, 6H), 3.44 (d, $^2J_{HH}$ = 15 Hz, methylene, 2H), 2.87 (s, N*Me*, 6H), 2.39 (s, Ph−*Me*, 6H), 2.20 (s, Ph−*Me*, 6H), 1.25 (s, CMe_3, 18H), 1.06 (s, CMe_3, 18H). ^{13}C NMR for **Ib** (δ, C_6D_6): 187.5, 162.8, 158.8, 138.7, 138.1, 132.1, 131.1, 130.2, 129.5, 128.8, 126.3, 125.2 (phenyl carbon), 57.8 (N*Me*, J_{CH} = 130 Hz), 46.1 (Ph−*Me*, J_{CH} = 130 Hz), 35.0 (*C*Me$_3$), 30.3 (C*Me*$_3$, J_{CH} = 125 Hz), 29.5 (C*Me*$_3$, J_{CH} = 125 Hz), 27.9 (methylene, J_{CH} = 126Hz), 21.4 (N*Me*, J_{CH} = 127 Hz). IR (KBr pellet of **Ib**): 2980 m, 2935 m, 2895 m, 2845 m, 2756 m, 1580 w, 1560 w, 1540 w, 1500 w, 1440 s, 1430 vs, 1380 m, 1350 m, 1320 w, 1280 w, 1250 sh, 1230 vs, 1140 s, 1120 s, 1100 m, 1030 m, 940 s, 915 s, 890 m, 880 s, 850 s, 840 vs, 790 s, 760 w, 740 w, 680 w, 560 s, 500 w, 480 w cm^{-1}. Anal. Calcd: C, 62.76; H, 7.53; N, 2.92. Found: C, 62.31; H, 7.32; N, 2.91. ^{1}H NMR for **Ic** (δ, C_6D_6): 7.10 (s, aromatic protons, 4H), 7.07 (s, aromatic protons, 4H), 5.36 (d, $^2J_{HH}$ = 15 Hz, methylene, 2H), 4.37 (s, N*Me*, 6H), 3.73 (d, $^2J_{HH}$ = 15 Hz, methylene, 2H), 2.09 (s, Ph−*Me*, 12H), 1.69 (s, C*Me*$_3$, 36H), 1.55 (s, N*Me*, 6H). ^{13}C NMR for **Ic** (δ, C_6D_6): 154.4, 140.2, 129.9, 129.8, 128.5, 126.5 (phenyl carbon), 58.7 (N*Me*, J_{CH} = 130 Hz), 39.1 (Ph−*Me*, J_{CH} = 130 Hz), 35.7 (*C*Me$_3$), 30.4 (methylene, J_{CH} = 126 Hz), 30.0 (C*Me*$_3$, J_{CH} = 126 Hz), 21.0 (N*Me*, J_{CH} = 127 Hz). IR (KBr pellet of **Ic**): 2985 m, 2940 m, 2845 m, 2785 w, 1553 m, 1460 s, 1377 s, 1302 m, 1217 w, 1173 m, 1156 m, 1115 w, 1079 w, 1069 w, 1026 m, 1003 s, 982 s, 858 m, 824 w, 795 m, 756 s, 721 vs, 704 vs, 689 s, 673 s, 637 w, 615 w, 590 w, 494 m cm^{-1}.

$W_2(\mu\text{-}H)(\mu\text{-}NMe_2)(\eta^2\text{-}O\sim\sim CH_2\sim\sim O)(\eta^3\text{-}O\sim\sim CH\sim\sim O)(NMe_2)(HNMe_2)$, 2. A solution of 2,2′-methylene-bis(6-*tert*-butyl-4-methylphenol) (0.321 g, 0.95 mmol) in pentane (10 mL) and diethyl ether (10 mL) was added to $W_2(NMe_2)_6$ (0.300 g, 0.475 mmol) in a hexane solution (10 mL) at room temperature. On mixing, the solution changed from yellow to dark black red. The solution was allowed to stand at room temperature for 12 h to yield black square platelike crystals of **2**. The solvent was removed by cannula, and the crystals were washed with cold hexane and diethyl ether and dried in vacuo. **2**·Et_2O was isolated (0.419 g, 75% yield). ^{1}H NMR for **2**·Et_2O (δ, C_6D_6): 11.54 (s, $^1J_{WH}$ = 129, 95 Hz), 7.80 (s, aromatic protons 2H), 7.20 (s, aromatic protons, 2H), 7.12 (s, aromatic protons, 4H), 6.98 (m, aromatic protons 2H), 5.10 (d, $^2J_{HH}$ = 15 Hz, methylene), 4.80 (s, 1H), 4.70 (s, 3H), 4.45 (s, 3H), 4.12 (d, $^2J_{HH}$ = 15 Hz, methylene), 3.86 (s, 3H), 3.31 (s, 3H), 3.26 (q, 4H), 3.15 (s, 3H), 2.32 (s, 6H), 2.13 (s, 3H), 2.16 (s, 6H), 1.88 (m, 36H), 1.13 (t, 6H). IR (KBr pellet): 3220 w, 3040 w, 2950 vs, 2910 vs, 2860 s, 2780 w, 1550 w, 1480 m, 1460 s, 1450 s, 1430 vs, 1405 s, 1380 m, 1370 m, 1350 m, 1290 m, 1280 m, 1245 vs, 1220 s, 1200 vs, 1180 s, 1160 m, 1140 m, 1120 m, 1110 m, 1030 w, 1010 s, 950 s, 920 s, 895 s, 880 s, 850 s, 820 vs, 800 m, 790 s, 780 s, 765 s, 750 w, 700 w, 660 s, 650 s, 610 s, 550 s, 535 m, 510 m, 450 m cm^{-1}. Anal. Calcd: C, 54.85; H, 7.18; N, 3.42. Found: C, 54.41; H, 7.34; N, 3.27.

$W_2(NMe_2)_2(\eta\text{-}O\sim\sim CH_2\sim\sim O)_2$, 3. A 30 mL Schlenk flask was charged with $W_2(NMe_2)_6$ (1.08 g, 1.7 mmol) and 2,2′-methylenebis-(6-*tert*-butyl-4-methylphenol) (1.160 g, 3.40 mmol), and 20 mL of toluene was added via cannula. A black-red solution formed. The solution then was stirred for 5 h, and the volatile components were removed under dynamic vacuum with slight warming. The residue was washed with 10 mL of cold hexane in two portions and dried *in vacuo*. A pure brown solid was obtained (1.20 g, 62% yield). ^{1}H NMR for **3** (δ, C_6D_6): 7.10 (s, aromatic protons, 4H), 6.95 (s, aromatic protons, 4H), 4.76 (d, $^2J_{HH}$ = 15 Hz, methylene, 2H), 4.41 (s, N*Me*, 6H), 3.76 (d, $^2J_{HH}$ = 15 Hz, methylene, 2H), 2.09 (s, Ph−*Me*, 12H), 1.64 (s, C*Me*$_3$, 36H), 1.59 (s, N*Me*, 6H). ^{13}C NMR for **3** (δ, C_6D_6): 152.7, 140.4, 130.1, 129.4, 129.3, 126.8 (phenyl carbon), 60.1 (N−*Me*, J_{CH} = 130 Hz), 36.4 (Ph−*Me*, J_{CH} = 130 Hz), 35.5 (*C*Me$_3$), 30.6 (methylene, J_{CH} = 126 Hz), 30.1 (C*Me*$_3$, J_{CH} = 126 Hz), 20.9 (N*Me*, J_{CH} = 127 Hz). IR (KBr pellet): 3180 w, 3040 w, 2940 s, 2900 s, 2845 s, 2760 w, 1750 w, 1580 vs, 1469 m, 1431 s, 1425 w, 1390 w, 1290 w, 1230 m, 1219 s, 1200 s, 1130 m, 1120 w, 1090 w, 947 m, 866 m, 835 m, 805 m, 780 m, 644 w, 573 w, 543 w cm^{-1}. Anal. Calcd: C, 53.01; H, 6.40; N, 2.47. Found: C, 52.43; H, 6.21; N, 2.47.

$W_2(\mu\text{-}H)(\mu\text{-}NMe_2)(\eta^2\text{-}O\sim\sim CH_2\sim\sim O)(\eta^3\text{-}O\sim\sim CH\sim\sim O)(NMe_2)(py)$, 4. $W_2(NMe_2)_2(\eta\text{-}O\sim\sim CH_2\sim\sim O)_2$ (0.1 g, 0.09 mmol) was suspended in 15 mL of hexane and 0.2 mL of pyridine. The solid was then dissolved in the hexane solution, and the color changed from brown to black. The solution was allowed to stand for 12 h, and black cubic crystals were isolated by decanting the solvent (0.083 g, 78% yield). ^{1}H NMR for **4** (δ, C_6D_6): 11.02 (s, $^1J_{WH}$ = 127, 90 Hz), 8.55, 7.63, 7.21, 7.01, 6.76 (aromatic protons), 5.30 (d, $^2J_{HH}$ = 15 Hz, methylene), 4.88 (s, 1H), 4.65 (s, 3H), 4.06 (s, 3H), 4.00 (d, $^2J_{HH}$ = 15 Hz, 1H), 3.31 (s, 3H), 3.20 (s, 3H), 2.26 (s, 3H), 2.20 (s, 3H), 2.15 (s, 3H), 2.10 (s, 3H), 1.67 (s, 9H), 1.45 (s, 9H), 1.36 (s, 9H), 1.16 (s, 9H). IR (KBr pellet): 3140 w, 3025 w, 2975 s, 2900 s, 2813 s, 2800 s, 2765 w, 1684 w, 1595 m, 1553 m, 1460 s, 1377 s, 1302 m, 1217 m, 1173 m, 1156 m, 1115 w, 1078 w, 1070 w, 1026 m, 1003 s, 982 s, 905 w, 900 w, 858 m, 810 w, 805 w, 795 m, 756 s, 721 vs, 701 vs, 689 s, 673 s, 637 m, 615 m, 590 m, 494 m cm^{-1}.

The Equilibrium 4 ⇌ 3 + Pyridine. **4** (6.5 mg) was dissolved in 0.661 g of benzene-d_6 in a J. Young NMR tube. The sample was placed in the NMR probe and the equilibrium monitored via NMR spectroscopy at various temperatures. The integration of methylene protons assignable to **3** and **4** were used for the equilibrium calculation. The probe temperature was calibrated with ethylene glycol. The K_{eq} (mole L^{-1}) values at different temperatures are as follows: 10 °C, 2.10 × 10^{-6}; 22 °C, 4.16 × 10^{-6}; 31 °C, 7.20 × 10^{-6}; 41 °C, 1.76 × 10^{-5}; 50 °C, 3.89 × 10^{-5}.

Ib to Ic Rearrangement. The rearrangement was performed by dissolving **Ib** (10 mg) in 0.5 mL of benzene-d_6 that contained various concentration of pyridine in a J. Young NMR tube. The samples were heated to 110 °C in a constant thermo-bath and monitored by NMR spectroscopy. The integration of methylene protons associated with **Ib** and **Ic** were used for the concentration calculation. The following k_{obs} (s^{-1}) were obtained: [py] = 2.62 M, k_{obs} = 3.73 × 10^{-4}; [py] = 1.51 M, k_{obs} = 1.36 × 10^{-4}; [py] = 0.91 M, k_{obs} = 7.32 × 10^{-5}; [py] = 0.60 M, k_{obs} = 4.96 × 10^{-5}; [py] = 0.37 M, k_{obs} = 3.73 × 10^{-5}.

The second part of this rearrangement measurement was performed by dissolving 10 mg of **Ib** in 0.5 mL of benzene-d_6 that contained 0.37 M of pyridine. Five individual measurement were performed and the integration of methylene protons was used for the concentration calculation. The following k_{obs} (s^{-1}) and k values were obtained through this measurement: 110 °C, k_{obs} = 4.52 × 10^{-5}, k = 3.30 × 10^{-4}; 100 °C, k_{obs} = 2.09 × 10^{-5}, k = 1.53 × 10^{-4}; 90 °C, k_{obs} = 1.03 × 10^{-5}, k = 7.49 × 10^{-5}; 80 °C, k_{obs} = 5.12 × 10^{-6}, k = 3.74 × 10^{-5}; 75 °C, k_{obs} = 3.07 × 10^{-6}, k = 2.24 × 10^{-5}.

(22) González, G.; Martinez, M.; Esteran, F.; Garcia-Bernabé, A.; Lahuerta, P.; Peris, E.; Ubeda, M. A.; Diaz, M. R.; Garcia-Granda, S.; Tejerina, B. *New J. Chem.* **1996**, *20*, 83.
(23) Miller, R. L.; Lawler, K. A.; Bennett, J. L.; Wolczanski, P. T. *Inorg. Chem.* **1996**, *35*, 3242.
(24) M = Mo ref. 11; W = W: Chisholm, M. H.; Martin, J. D. *Inorg. Synth.* **1992**, *29*, 137.

Table 9. Summary of Crystal Data

	Ib	**Ic**·$3C_6H_6$	**2**·Et_2O	**4**·$^1/_2$py
empirical formula	$C_{50}H_{72}N_2O_4Mo_2$	$C_{68}H_{90}N_2O_4Mo_2$	$C_{56}H_{89}N_3O_5W_2$	$C_{66}H_{72}N_3O_4W_2$·1/2C_5H_5N
space group	*C*2/*c*	$P2_1/c$	*Pbca*	*C*2/*c*
temp (°C)	−173	−170	−170	−172
a (Å)	24.999(4)	15.229(2)	23.285(3)	21.834(13)
b (Å)	11.283(1)	16.947(2)	25.800(3)	16.952(9)
c (Å)	17.551(2)	24.950(3)	18.364(2)	31.332(18)
β (deg)	90.30(10	106.96(1)		110.04(2)
Z (molecules/cell)	4	4	8	8
V (Å^3)	4950.57	6158.94	11031.98	10895.00
d_{calcd} (g cm^{-3})	1.284	1.285	1.508	1.516
wavelength (Å)	0.71069	0.71069	0.71069	0.71069
linear abs coeff (cm^{-1})	5.343	4.426	43.024	43.551
R(*F*)	0.0478	0.0471	0.0485	0.0618
R_w(*F*)	0.0584	0.0457	0.0444	0.0579
max d/s for last cycle	0.02	0.01	0.038	0.11

Crystallographic Studies. General operating procedures and a listing of programs have been given previously.[25] A summary of crystal data is given in Table 9.

Ib. A crystal of suitable size was mounted using silicone grease and transferred to a goniostat where it was cooled to −173 °C for characterization and data collection. A systematic search of a limited hemisphere of reciprocal space revealed symmetry and systematic absences corresponding to two monoclinic space groups *C*2/*c*, and *Cc*. An initial choice of the centrosymmetric one was confirmed by the successful solution of the structure.

The structure was solved by a usual combination of direct method (MULTAN78) and Fourier techniques. The Mo atom positions were obtained from an initial *E*-map, and the remainder of the non-hydrogen atoms were found in subsequent iterations of least-squares refinement of the non-hydrogen atoms, hydrogen atoms were included in the calculated positions. 283 parameters were refined using 2873 reflections with $F(hkl) > 3\sigma F$ to the final *R*-factor 4.8%.

A final difference Fourier was featureless, with the largest peak being 0.65 e/Å^3.

Ic. A suitable crystal was affixed to the end of a glass fiber using silicon grease and transferred to the goniostat where it was cooled to −170 °C.

After the crystal was transferred to the goniostat, a systematic search of a limited hemisphere of reciprocal space was used to determine that the crystal possessed monoclinic symmetry and systematic absences corresponding to the unique space group $P2_1/c$. Subsequent solution and refinement confirmed this choice.

Data were collected by using a standard moving crystal-moving detector technique with fixed backgrounds at each extreme of the scan. Data were corrected for Lorentz and polarization effects and equivalent reflections were the averaged. The structure was readily solved using direct methods (SHELXTL-PC) and Fourier techniques. Hydrogen atoms were placed in fixed calculated positions and were included as fixed contributors in the final cycles of refinement. Three independent molecules of benzene solvent were present in the cell and were well ordered.

A final difference Fourier was featureless, the largest peak lying at one of the metal positions (2.1 e/Å^3).

2. A crystal of suitable size was mounted in a nitrogen atmosphere glovebox by using silicone grease, and it was then transferred to a goniostat where it was cooled to −170 °C for characterization and data collection. A systematic search of a limited hemisphere of reciprocal space revealed a primitive orthorhombic cell. Following complete data collection, the conditions $k = 2n$ for $0kl$, $l = 2n$ for $h0l$, and $h = 2n$ for $hk0$ uniquely determined space group *Pbca*. After correction for absorption, data processing gave a residual of 0.039 for the averaging for 2558 unique intensities which had been observed more than once. Four standards measured every 400 data showed no significant trends.

The structure was solved by using a combination of direct methods (MULTAN78) and Fourier techniques. The tungsten positions were obtained from an *E*-map. The remaining non-hydrogen atoms were obtained from subsequent iterations of least-squares refinement and difference Fourier calculations. Some of the hydrogen atoms, including the hydride atom, H(1), were weakly observed. All hydrogen atoms except H(1) were included in fixed calculated positions with thermal parameters fixed at one plus the isotropic thermal parameters of the atom to which they were bonded.

In the final cycles of refinement, the non-hydrogen atoms were varied with anisotropic thermal parameters and H(1) was varied with an isotropic thermal parameter to a final $R(F) = 0.0485$. The largest peak in the final difference map was a tungsten residual of 1.3 e/Å^3.

In addition to the molecule of interest, the asymmetric unit contains one molecule of diethyl ether which had been used as solvent. All remaining plots contain only the molecule of interest.

4. The sample consisted of numerous needle-shaped, transparent crystals whose cross section was diamond shaped. Several of the crystals examined were found to be either twinned or split. A nearly equidimensional fragment was cleaved from the center of a nearly perfectly formed needle and was affixed to the end of a glass fiber using silicone grease. It was then transferred to the goniostat where it was cooled to −172 °C for characterization and data collection. Examination indicated that the selected sample was not twinned or split.

A systematic search of a limited hemisphere of reciprocal space located a set of diffraction maxima with monoclinic symmetry and systematic absences corresponding to space group *Cc* or *C*2/*c*. Subsequent solution and refinement confirmed the centrosymmetric space group *C*2/*c*.

The data were collected by using a standard moving crystal-moving detector technique with fixed backgrounds at each extreme of the scan. Data were corrected for Lorentz and polarization effects, and equivalent reflections were averaged after applying an absorption correction.

The structure was readily solved by direct methods (MULTAN78) and Fourier techniques. Hydrogen atoms were clearly visible for much of the molecule in a difference Fourier phased on the non-hydrogen atoms and were placed in fixed idealized positions for the final cycles of refinement. A peak located in the position expected for the hydride was located (H(A)) and was also included in the final cycles as a fixed atom contributor. A disordered solvent molecule was also present, lying on the 2-fold axis t 0, *y*, $^1/_4$. When the non-hydrogen atoms were allowed to vary anisotropically, several converged to nonpositive definite values, and the overall residual did not significantly drop. For this reason only the metal atoms were refined anisotropically in the final cycles.

A final difference Fourier was featureless, the largest peak (2.4 e/Å^3) being adjacent to the tungsten atoms.

Acknowledgment. We thank the National Science Foundation and the Department of Energy, Office of Basic Sciences, Chemistry Division, for financial support and Dr. M. Pagel for assistance with the MM calculations.

Supporting Information Available: Tables giving a summary of data collection, atomic coordinates, and complete listings of bond distances and angles and VERSORT drawings for **Ib**, **Ic**, **2**, and **4** (57 pages). Ordering Information is given on any current masthead page.

(25) Chisholm, M. H.; Folting, K.; Huffman, J. C.; Kirkpatrick, C. C. *Inorg. Chem.* **1984**, *23*, 1021.

IC961429N